

This is the accepted manuscript of the contribution published as:

Zhang, R., Neu, **T.R.**, Blanchard, V., Vera, M., Sand, W. (2019):
Biofilm dynamics and EPS production of a thermoacidophilic bioleaching archaeon
New Biotech. **51** , 21 – 30

The publisher's version is available at:

<http://dx.doi.org/10.1016/j.nbt.2019.02.002>

Biofilm dynamics and EPS production of a thermoacidophilic bioleaching archaeon

Ruiyong Zhang^{a, b}, Thomas R. Neu^c, Véronique Blanchard^d, Mario Vera^e, and Wolfgang Sand^{b, f, g*}

^aFederal Institute for Geosciences and Natural Resources, Hannover, Germany

^bBiofilm Centre, Universität Duisburg-Essen, Essen, Germany

^cDepartment of River Ecology, Helmholtz Centre for Environmental Research – UFZ, Magdeburg, Germany

^dInstitute of Laboratory Medicine, Charité Medical University, Berlin, Germany

^eInstitute for Medical and Biological Engineering, Schools of Engineering, Medicine and Biological Sciences. Department of Hydraulic and Environmental Engineering, School of Engineering. Pontificia Universidad Católica de Chile, Santiago, Chile

^fCollege of Environmental Science and Engineering, Donghua University, Shanghai, China

^gTU Bergakademie Freiberg, Freiberg, Germany

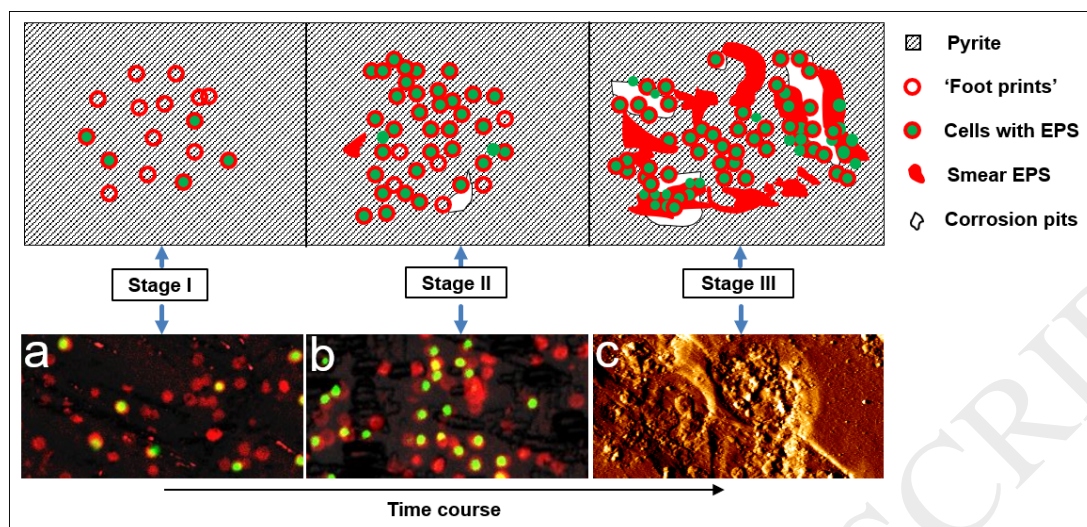
* *Correspondence:*

wolfgang.sand@uni-due.de

Graphical abstract

A model for the biofilm growth by *Acidianus* sp. DSM 29099 on pyrite is given. In the first stage (24-48 h), reversible attachment is possible. It is accompanied by the production of adhesive compounds on the mineral surface. Biofilm formation on pyrite by *Acidianus* sp.

DSM 29099 is a dynamic process accompanied by formation of pits and production of adhesive compounds, which after cell detachment remain as footprints.



Highlights

- *In situ* visualization of biofilms and EPS of thermoacidophilic archaea on pyrite
- Direct detection of footprints of cells of *Acidianus* sp. DSM 29099
- EPS extraction and analysis of *Acidianus* in bioleaching environments
- Suggestion of a model for biofilm formation by *Acidianus* sp.

Abstract

Bioleaching of metal sulfides represents an interfacial process where biofilm formation is important in the initial steps of this process. In technical applications of bioleaching, such as reactor leaching in the temperature range of 50 up to 90 °C and also in (self-heating) heaps,

thermophilic archaea play an important role and often are the leaching organisms of choice. Nevertheless, to date there is little information available on the interactions between thermoacidophilic archaea and their natural mineral substrates such as pyrite. Especially for extracellular polymeric substances (EPS) of archaea and their biofilms in bioleaching environments information is rather limited. The present work focused on investigations of biofilm dynamics and EPS production of the thermoacidophilic archaeon *Acidianus* sp. DSM 29099 under bioleaching conditions. The results show that biofilms are dispersed non-homogeneously on pyrite. Large parts of the pyrite surfaces remain free of cells. Cell detachment from pyrite results in microbial “footprints” which, based on lectin binding assays, consist of mannose, glucose and fucose containing compounds. A monolayer biofilm develops on pyrite after 2-4 days of incubation. In addition, the pyrite surface is covered with a layer of organic compounds. EPS analysis indicates the presence of proteins, polysaccharides and uronic acids, the composition of which varies according to substrate and lifestyle (i.e. planktonic, biofilm cells). This report provides insight into EPS and biofilm characteristics of thermophilic archaea and improves understanding of the mineral-microbial-biofilm interfacial interactions in extreme environments. Moreover, the results on interaction dynamics of archaeal microbial consortia will facilitate the understanding of thermophilic bioleaching.

List of Abbreviations

acid mine drainage/acid rock drainage (AMD)/(ARD)

Aleuria aurantia lectin (AAL)

atomic force microscopy (AFM)

bovine serum albumin (BSA)

cation exchange resin (CER)

Concanavalin A lectin (Con A)

confocal laser scanning microscopy (CLSM)
epifluorescence microscopy (EFM)
extracellular DNA (eDNA)
extracellular polymeric substances (EPS)
fluorescence lectin-barcoding (FLBC)
fluorescent lectin-binding analysis (FLBA)
glucose-6-phosphate dehydrogenase (G6PDH)
metal sulfide (MS)
N-acetyl galactosamine (GalNAc)
N-acetyl glucosamine (GlcNAc)
numerical aperture (NA)
reduced inorganic sulfur compounds (RISCs)
room temperature (RT)
scanning electron microscopy (SEM)
standard deviations (\pm SD)
terminal restriction fragment polymorphism (T-RFLP)
transmission electron microscopy (TEM)
yeast extract (YE)

Keywords: bioleaching; biofilm dynamics; extracellular polymeric substances; thermoacidophilic archaea; confocal laser scanning microscopy

Introduction

Bioleaching is applied worldwide for metal recovery from low grade ores, mineral concentrates or waste materials [1, 2]. It is recognized as being one of the most eco-friendly technologies for metal recovery. Bioleaching also occurs naturally and may result in serious environmental problems, i.e. acid mine drainage (AMD) or acid rock drainage (ARD). The microorganisms responsible for mineral dissolution are mainly members of the bacterial phyla *Proteobacteria*, *Nitrospira*, *Actinobacteria* and *Firmicutes*, plus representatives of *Euryarchaeota* and *Crenarchaeota* [3]. These microbes in general can generate the oxidation reagent iron(III) and/or protons for mineral dissolution through oxidation of iron(II) or reduced inorganic sulfur compounds (RISCs) [4]. The order *Sulfolobales*, which includes thermoacidophiles *Sulfolobus* (*S.*) sp., *Acidianus* (*A.*) sp. and *Metallosphaera* (*M.*) sp., has been proven to enhance metal extraction from recalcitrant mineral sulfides, especially in heap or dump operations [5, 6].

Nearly all microorganisms are able to grow as self- or surface-associated multi-cellular communities known as biofilms. After cell attachment to a surface, the production of extracellular polymeric substances (EPS) begins. These contribute significantly to the organization and structural integrity of biofilm communities [7]. EPS in general are composed of carbohydrates, proteins, lipids, and nucleic acids [8]. They may be present in planktonic growth forms (e.g. flocs, cell aggregates) or within surface-associated biofilms. Depending on the way EPS are removed and according to their association with the cell surface two types are defined: 'loosely bound / colloidal EPS' and 'tightly bound / capsular EPS' [9]. Capsular EPS are tightly bound to the cell surface and their extraction normally needs an extensive physical and/or chemical treatment. 'Colloidal EPS' are loosely bound to the cell surfaces and can be easily removed from the cells (e.g. by centrifugation or washing) [9]. Attachment, biofilm

formation and the presence of EPS are of fundamental importance for microbially caused/induced mineral dissolution [4]. Cell-mineral interactions of mesophilic and moderate thermophilic bacteria regarding the change of bacterial lifestyle and EPS composition in biomining environments have been reported [10, 11]. The EPS concept and their analysis in the bioleaching field were first introduced in 1998 [12], as bioleaching bacteria like *Acidithiobacillus* were thought to be the most important microorganisms in bioleaching. Later, it was observed that archaea may contribute as much as their counterparts (bacteria) in bioleaching process [13, 14]. In technical applications of bioleaching like reactors leaching in the temperature range of 50 up to 90 °C as well as in (self-heating) heaps, archaea may play an important role and are often the leaching organisms of choice. To date, only a few studies on EPS components of thermoacidophilic archaea are available. By extraction with a cation exchange resin (CER) it was shown that proteins and carbohydrates are the major components in the EPS of *S. solfataricus* P2 grown on tryptone, N-Z-amine or glucose [15]. Furthermore, it was shown that carbohydrates and proteins are the major constituents and DNA a minor component in the *S. acidocaldarius* EPS [16]. These studies were focused on the EPS production by cells grown on soluble organic substrates. The attachment, biofilm features, and EPS polymers of acidophilic archaea on their solid substrates, e.g. elemental sulfur as well as metal sulfides, have been rarely reported.

Recently, we have applied fluorescence lectin-barcoding (FLBC) and fluorescent lectin-binding analysis (FLBA) [17] to study biofilms and EPS glycoconjugates of three pyrite leaching archaeal species *F. acidiphilum* BGRM4, *Acidianus* sp. DSM 29099 and *S. metallicus* DSM 6482^T. Various glycoconjugates containing monosaccharides such as fucose, glucose, galactose, mannose, N-acetyl glucosamine (GlcNAc) and N-acetyl galactosamine (GalNAc) were detected [18]. Tightly-bound EPS of cells of the sulfur-grown *S. metallicus*^T were shown

to be composed of proteins and carbohydrates. By contrast, the loosely bound EPS contained mainly carbohydrates. In addition, extracellular DNA (eDNA) was found in the biofilm matrix [19].

In a previous study it was shown that *S. metallicus*^T and *A. copahuensis* negatively influence each other during initial attachment and pyrite dissolution. In addition, physical contact between the two species seems to exist, as revealed by specific lectins able to bind to single species within the mixed cultures [20]. A pre-colonization with cells of *Sb. thermosulfidooxidans* enhanced the pyrite bioleaching efficiency of *Acidianus* sp. DSM 29099 [21]. Nevertheless, there is little information available on the interactions between thermoacidophilic archaea and their natural substrates such as pyrite. Especially for archaeal EPS and biofilms in bioleaching environments data are rather limited [8, 22].

In this report, the aim was to characterize the initial cell attachment, biofilm development and EPS production of *Acidianus* sp. DSM 29099 on pyrite. Several microscopic techniques including atomic force microscopy (AFM) epifluorescence microscopy (EFM), confocal laser scanning microscopy (CLSM), scanning electron microscopy (SEM) and transmission electron microscopy (TEM) were used to study cell attachment and biofilm formation. AFM combined with EFM takes advantages of high resolution of surface structure/morphology and identification of materials of biological origin [23]. CLSM (upright) with the freedom of mounting specimens combined with various fluorescent stains allows 3d multi-channel *in situ* visualization of biofilms in fully-hydrated conditions [24]. By using conventional spectrophotometric methods as well as FLBC and FLBA the EPS composition was studied comparatively for planktonic and biofilm cells grown on iron(II) ions or pyrite. Our study provides insights into attachment and EPS composition of *Acidianus* sp. DSM 29099 under

pyrite and chalcopyrite leaching conditions, thereby improving our understanding of the roles of thermoacidophilic archaea in high temperature leaching environments.

Materials and Methods

Strains and characterization

Acidianus sp. DSM 29099 was obtained from a hot spring in the Copahue–Caviahue region, Argentina. Cells were grown in basal salts medium (MAC medium) [25] with addition of yeast extract (YE, 0.02%). The initial pH of the medium was set to 1.8 using H₂SO₄ (5 M), where cells were grown on iron(II) ions (4 g/L) or on pyrite (10%), and pH 2.5 where cells were grown on elemental sulfur (S⁰, 10 g/L). The culture was run at 65 °C on a shaker at 120 rpm in the dark. Growth curves on iron(II) ions were conducted by measuring cell number, solution pH and iron concentrations at different intervals for 52 h.

Genomic DNA of *Acidianus* sp. DSM 29099 was extracted as previously described [26]. Briefly, cell pellets were suspended in 400 µL salt buffer (TE buffer: 0.4 M NaCl 10 mM Tris-HCl pH 8.0 and 2 mM EDTA pH 8.0). 44 µL of 20% SDS and 2 µL RNase A were added and mixed well. The samples were incubated at 65°C for 1 h, after which 300 µL of 6M NaCl was added. Samples were vortexed for 30 s at maximum speed. The supernatant was decanted after centrifugation at 17600 g for 30 min. An equal volume of isopropanol was added and after mixing well, the samples were stored at -20 °C overnight. The DNA pellet was washed with 70% ethanol and dissolved in 500 µL of dd H₂O. The 16S rDNA genes of *Acidianus* sp. DSM 29099 were amplified using archaeal primers as previously described [27]. The amplified 16S rRNA genes were cloned using the pGEM®-T vector system (Promega®). Ligation reactions were transformed in competent *E. coli* DH5α cells. Plasmids were isolated using Roti®-Prep

Plasmid MINI Kit (Carl Roth, Karlsruhe, Germany). DNA sequencing was performed by the Institute of Human Genetics, University Hospital Essen (Essen, Germany). The sequences were subjected to BLAST homology search (<http://www.ncbi.nlm.nih.gov/BLAST>). DNA-DNA hybridization was performed by the Identification Service of the Leibniz-Institute DSMZ (German Collection of Microorganisms and Cell Cultures GmbH, Braunschweig, Germany). *S. metallicus* 6482^T was obtained from DSMZ and maintained on pyrite and S⁰. Cells were cultivated at the same conditions as described for *Acidianus* sp. DSM 29099.

Mineral preparation and leaching experiments

Pyrite slices and grains were prepared and sterilized as described previously [28]. Chalcopyrite grains with a size of 50-200 µm were selected and washed with EDTA (0.1 M) and NaOH (0.4 M), treated with deionized water and acetone and heat-sterilized at 120 °C for 24 h under a N₂ atmosphere.

300-mL Erlenmeyer flasks containing 10 g pyrite grains, 100 mL MAC medium (pH 1.8) and 0.02% YE were inoculated with cells of *Acidianus* sp. DSM 29099 at an initial cell number of 1-2×10⁸ cells/mL. For comparison, pyrite bioleaching by the type strain *S. metallicus*^T was tested under the same growth conditions for 38 d. In addition, abiotic controls were performed. The loss of water due to evaporation at 65 °C was adjusted for by adding sterile water. Experiments were performed in duplicate. For determination of cell numbers, approximately 20 µL liquid samples were transferred to a Thoma Chamber (Hecht-Assistent) for cell count under a light microscope (Leica DM3000), in phase contrast mode with 400× magnification. The pH was measured using a digital pH meter (Model pH 537, WTW). For iron determination, liquid samples were withdrawn and filtered through polycarbonate filters (pore size 0.2 µm). Iron determination was using the phenanthroline method (according to DIN 38406-1).

Attachment tests

Attachment tests were performed according to previous reports [29, 30]. Briefly, mineral grains (pyrite or chalcopyrite) were incubated with pyrite-grown cells of *Acidianus* sp. DSM 29099 in 50 mL MAC medium under shaking at 120 rpm. The initial cell concentration was adjusted to $1-2 \times 10^8$ cells/mL. As a control, quartz was used to evaluate the non-specific cell attachment. Liquid samples of 0.5 mL were taken over a period of 6 h to determine the number of planktonic cells. The intervals for sampling were 0, 5, 10, 30, 60, 120 and 360 min. Cell numbers were determined as above. The number of attached cells was calculated by subtracting the number of remaining planktonic cells from the initial cell number inoculated.

Visualization of attachment and biofilm development on pyrite by CLSM

Staining for EPS glycoconjugates and cell nucleic acids was performed according to the previous study [18]. No fixation was needed as biofilm cells are electrostatically and mechanically fixed (adhesion to mineral and embedded in EPS matrix). For EPS glycoconjugates staining, pyrite grains or slices colonized with biofilm cells were withdrawn from shaking flasks at different intervals (1, 2, 4, 5, and 7 d) and were placed into a coverwell chamber 20 mm in diameter with 0.5 mm spacer or a 5 cm Petri dish (Molecular Probes or Thermo Fisher), respectively. Samples were washed with filter-sterilized tap water and incubated with 0.1 mg/mL lectins (Con A-TRITC or AAL-A488, Invitrogen) for 20 min at room temperature (RT). Stained samples were washed 3x with filter-sterilized tap water in order to remove unbound lectins, avoiding direct light exposure. Counter staining was with Syto 64 or SybrGreen. Stained samples were immediately examined *in situ* by CLSM using an upright microscope TCS SP5X, controlled by the LASAF 2.4.1 build 6384 (Leica,

Heidelberg, Germany). Fields of view were 150×150 µm, and more than 5 fields were checked for each sample and at least 3 spots from each sample were visualized. Images of Z-stacks were recorded. For visualization of surface topography and texture of pyrite CLSM in reflection mode was used. Auto-fluorescence of the samples/cells of *Acidianus* sp. DSM 29099 was tested by means of lambda scan, and resulted in very weak signals, thus auto-fluorescence was not an issue (not shown). Samples were examined using a 63× water immersible objective lens with a numerical aperture (NA) of 0.9. Depending on the fluorochrome application, image data sets were recorded at the following settings:

- 1) excitation 490 nm – emission 485-495 nm (reflection), 510-580 nm (SybrGreen), and excitation 557 nm, emission 580-650 nm (Con A-TRITC);
- 2) excitation 475 nm – emission 470-480 nm (reflection), 500-580 nm (AAL-A488);
- 3) excitation 490 nm – emission 485-495 nm (reflection), 500-580 nm (AAL-A488), and excitation 599 nm, emission 620-720 nm (Syto 64).

Digital image analysis

Digital image analysis was performed using an extended version of the software ImageJ (v1.50i) and IMARIS version 8.1.2 (Bitplane AG, Zurich, Switzerland). In some cases, contrast and brightness were slightly adjusted with tools in Photoshop CS6. To reflect the biofilm density of *Acidianus* sp. DSM 29099 on pyrite, surface coverage of cells and biofilms on pyrite surface were calculated by ImageJ.

Scanning electron microscopy

Planktonic cells grown on pyrite for 7 d were withdrawn and collected on a polycarbonate filter (0.2 µm) by filtration. Pyrite slices and the polycarbonate filter with cells were rinsed with

deionized water and dehydrated successively with increasing concentrations of acetone (60%, 80% and 90%), and stored overnight at 4 °C in 90% acetone. Samples were subjected to critical-point drying and coated with graphite and gold. Specimens were examined with a JEOL JSM-6330F microscope, FE-SEM at 10 kV.

Transmission electron microscopy

For cell morphology observation, 1 mL of cell cultures grown on pyrite or sulfur for 7 d were withdrawn and briefly centrifuged at 400 g for 5 s to remove pyrite grains. Subsequently, 10 μ L drops of the cell culture were placed on Parafilm® sheets. Formvar® copper coated grids were placed on these cell culture drops and cells were allowed to adsorb for 10 min; the grids were then air-dried. Samples were observed using a TEM (Jeol 1400, Japan) at an accelerating voltage of 80 kV.

Atomic force microscopy and epifluorescence microscopy

The AFM and EFM setups were reported in our previous studies [29]. Briefly, a NanoWizard II AFM (JPK Instruments) in contact mode and an upright epifluorescence microscope (AxioImager A1m; Zeiss, Germany) with a $\times 100$ water-immersible objective (Achromplan; numerical aperture 1.0; working distance, 0.97 mm) without using coverslips were combined using the BioMaterialWorkstation (JPK Instruments). CSC37-A (Mikromasch, Estonia) probe was used and the following parameters were chosen for scanning: typical length, 250 μ m; width, 35 μ m; thickness, 2 μ m; resonance frequency, 41 kHz; and nominal force/spring constant, 0.65 N/m. Each AFM image consists of 512 \times 512 or 1024 \times 1024 pixels.

Planktonic cells grown on sulfur for 7 d were withdrawn and fixed on glass slides by evaporation at RT. Cell morphology was directly observed via AFM; Pyrite slices were rinsed

with sterile MAC medium and deionized water. Cells attached to pyrite slices and their EPS glycoconjugates were stained by Syto 9 (Invitrogen) and by Con A-TRITC (Invitrogen). Stained samples were dried at RT and visualized by EFM (Zeiss, Germany) combined with AFM for the investigation of cell morphology and distribution on the surfaces of pyrite coupons. With this combination, a sample can be visualized at the same location under both microscopes with only a few micrometers' deviation, as previously described [37]. At least 3 different spots (approximately $100 \times 100 \mu\text{m}$) from each sample were checked and recorded by combined AFM and EFM.

EPS extraction and analysis

After 7 d incubation, planktonic cells ($\sim 9 \times 10^8$ cells/mL) grown on pyrite and pyrite grains with attached biofilm cells were separated by filtration through sterile Whatman filter paper. Planktonic cells ($\sim 8 \times 10^7$ cells/mL) of *Acidianus* sp. DSM 29099 grown on iron(II) ions for 3 d or on pyrite were collected by centrifugation at 11300 g for 15 min. Cell pellets were washed with MAC medium and freeze-dried (ALPHA 2-4 LSC, -80°C). The supernatant was filtered through polycarbonate filters (GTTB, $\text{Ø}2.5$ cm, $0.2 \mu\text{m}$ pore size, Millipore®) to remove remaining planktonic cells. These cell-free supernatants (containing the 'colloidal EPS' fraction) were dialyzed using a cellulose membrane (cutoff 3.5 KDa) against deionized water at 4°C for 48 h. Dialyzed colloidal EPS solutions were freeze-dried. Capsular EPS were extracted from cell pellets using 20 mM EDTA as previously described [31]. The pyrite grains with biofilm cells were incubated with 20 mM EDTA at 4°C with shaking at ~ 260 rpm for 6 h to extract EPS. The extraction was repeated 3x and the resulting solutions were centrifuged, filtered and dialyzed as described above.

Carbohydrate determination was performed by the phenol-sulfuric acid method with glucose as standard [32]. Uronic acids were estimated using glucuronic acid as standard [33]. Protein concentration was analysed with bovine serum albumin (BSA) as standard [34]. Cell lysis was estimated by measuring glucose-6-phosphate dehydrogenase (G6PDH) activity [35].

For sulfate determination, EPS samples were hydrolyzed in 1 M HCl for 2 h at 80 °C. Afterwards, the hydrolysates were evaporated at 65 °C to dryness. The dried samples were then dissolved in Milli-Q water. Sulfate was determined by indirect atomic absorption spectroscopy [36]. EPS determinations were performed in duplicate. EPS from planktonic cells were normalized by cell number and EPS from biofilms by amount of pyrite. Mean values are given with standard deviations (\pm SD).

Results and Discussion

Strain characterization and identification

The archaeal isolate originates from the Caviahue–Copahue volcanic system, Argentina, and has been deposited in the DSMZ under number 29099. Cells are non-motile and occur mostly as single cells, if grown with S^0 , iron(II) ions or pyrite. As shown in **Figure 1**, they are irregular spheres with a diameter of 0.9-2 μ m. Cell surfaces seem to be slimy and uneven, possibly due to superficial EPS (as indicated by arrows in Figure 1). In addition, wrinkled and lobed surfaces are clearly visible in both, AFM and SEM images (Figure 1A and B). These characteristics fit the general features of the order *Sulfolobales*. TEM observations demonstrate the presence of an EPS matrix, which forms a discontinuous coating over the cell surface, and in some locations EPS forms bridges linking cells (Figure 1C).

The 16S rDNA genes of *Acidianus* sp. DSM 29099 were cloned and the sequences were deposited in GenBank (accession no. KJ921703). Sequence analysis revealed that this strain is phylogenetically affiliated to the newly defined, but not yet validly described species *A. copahuensis* DSM 29038 (99% similarity) [37]. DNA-DNA hybridization data also strongly suggest that strain *Acidianus* sp. DSM 29099 should be classified as *A. copahuensis*, since both strains share an 80.8% DNA-DNA similarity [38]. They share similar properties in morphology and physiology, e.g. both are capable of utilizing tetrathionate and galactose as energy substrates ([37]; Supplementary Table S1). Some distinguishing characteristics between strains *Acidianus* sp. DSM 29099 and *A. copahuensis* DSM 29038 exist, e. g. strain DSM 29099 has an optimum growth temperature of 65 °C and DSM 29038 optimal growth T° of 75 °C. In addition, expression of different EPS glycoconjugates was observed previously for the two strains by means of FLBA [20].

Growth and iron(II) ion oxidation

As shown in **Figure 2**, cells of *Acidianus* sp. DSM 29099 grew rapidly using iron(II) ion oxidation. Cell numbers reached a maximum 7×10^7 cells/mL after 30 h of cultivation. Meanwhile, cell growth was accompanied by a non-linear decrease of the iron(II) ion concentration, with 80% of total iron(II) ions oxidized within 30 h. This indicates the coupling of iron oxidation and cell growth. The cell yield was 2×10^{10} cells/g iron(II). This is comparable with that obtained for cultivation of *A. brierleyi* DSM 1651^T [39]. Cell numbers decreased rapidly after 36 h of cultivation, clearly due to the exhaustion of iron(II) ions. The culture pH kept increasing from 1.7 to 2.0. The approximate specific growth rate and maximal iron oxidation rate were 0.037/h and 113 mg/L·h, respectively. Abiotic control experiments showed that only ~5% of total iron(II) ions had been oxidized at the end of the test (not shown).

Pyrite leaching by Acidianus sp. DSM 29099

Pyrite oxidation by *Acidianus* sp. DSM 29099 was compared with the type strain of *S. metallicus*^T. As indicated in **Figure 3**, both strains had a similar leaching performance with 25 or 30 g/L of total iron leached after 38 d. The pyrite dissolution rate was approx. 14.9 and 12.4 mM pyrite/d for *Acidianus* sp. DSM 29099 or *S. metallicus*^T, respectively. Cell numbers of both strains increased within the first 15 d up to 1.3×10^9 and 1.1×10^9 cells/mL, respectively. Increased biomass was obtained when cells of *Acidianus* sp. DSM 29099 grew on pyrite compared to growth with iron(II) ions (Figures 2 and 3). The pyrite oxidation rate of *Acidianus* sp. DSM 29099 was 4 times higher than that of *A. brierleyi* [40], and up to 6 times higher than mesophiles such as *At. ferrooxidans* strain R1 or C-52 [41]. Microbes with high iron(II) oxidation rate can promote a rapid dissolution of pyrite or chalcopyrite [4]. In abiotic assays of pyrite leaching at 65 °C approximately 0.6 g/L of total iron were detected, which was much higher than for the assay at 37 °C (Supplementary Fig. S1). Thus, high temperature did result in an acceleration of abiotic pyrite dissolution, but to a limited extent. The abiotic pyrite leaching at 65 °C was negligible compared to bioleaching with *Acidianus* sp. DSM 29099.

Cell numbers of *S. metallicus*^T started to decrease rapidly after 22 d incubation, while total iron ions reached 9.7 g/L and pH 1.0, respectively. In contrast, the cell numbers of *Acidianus* sp. DSM 29099 remained stable until 38 d at approx. 1.3×10^9 cells/mL. It seems that cells of *Acidianus* sp. DSM 29099 possess a better resistance to high concentrations of iron ions and protons than those of *S. metallicus*^T. This observation is consistent with the previous report that *Acidianus* showed better adaptation than *S. metallicus* to bioleaching environments [42]. After 40 d of leaching, yellowish precipitates were detected in assays of both strains, although the

pH reached ~0.8 in both cases. These iron sulfate compounds may be jarosites, which can be formed at low pH (< 2) as observed by [40].

Initial attachment to pyrite

Data in **Figure 4** indicate that approximately 40% of *Acidianus* sp. DSM 29099 cell inoculum, pre-grown on pyrite, rapidly adhered to pyrite within the first 5 min. The maximum amount of cells attached to pyrite was 60% within 6 h incubation. Approximately 35% of the cells attached to chalcopyrite. This agrees with previous findings that attachment of acidophiles on surfaces is mineral-selective [30]. As expected, only a small proportion of cells (~10%) attached to quartz, which served as a negative control. Cells pre-cultivated with S^0 showed less attachment to pyrite compared to pyrite-grown cells (~40% in 6 h, not shown). Thus, pre-cultivation also has an influence on cell attachment of *Acidianus* sp. DSM 29099 [43].

It has been demonstrated that attachment of *A. manzaensis* to chalcopyrite is dependent on the presence of secondary minerals (e.g. bornite or covellite) and the microstructure of the chalcopyrite surface. Both iron and sulfur availability on a chalcopyrite surface will influence cell adsorption. However, the former has the larger influence on the cellular attachment [44]. The attachment of *M. hakonensis* was shown to be influenced by culture history and growth temperature [45]. In addition, cells formed denser biofilms on pyrite than on chalcopyrite [46]. In the current study, positive signals by AAL-A488 staining indicated EPS residues containing fucose in biofilms on pyrite but not on chalcopyrite (Supplementary Fig. S2). This is consistent with previous studies where cells of the same strains express different EPS glycoconjugates on different substrates [18].

Cellular appendages are presumably involved in the initial attachment of extremophilic archaea, such as *S. solfataricus*, *Halobacterium*, *Haloferax* or *Halorubrum* adhering to plastic or glass surfaces [47]. Fimbriae/cannulae-like appendages of *Acidianus* sp. DSM 29099 were sometimes visible in TEM images (Supplementary Fig. S3). Genes encoding flagellar assembly proteins are present in the genomes of *A. copahuensis* and *A. manzaensis* YN-25 [48].

Biofilm development on pyrite

Lectins such as Con A (Concanavalin A lectin) and AAL (*Aleuria aurantia* lectin) are often used to visualize EPS glycoconjugates and biofilms of leaching archaea, e.g. *F. acidiphilum* [18], *A. copahuensis* [43], *S. metallicus* [18], *M. hankonensis* [46] and the bacterium *At. ferrooxidans* [49]. Thus, these two lectins were chosen to monitor biofilm development of cells of *Acidianus* sp. DSM 29099. Our previous study indicated that biofilm cells of *Acidianus* sp. DSM 29099 could be localized by Sypro stains (protein staining), but staining by Sypro stains did not reflect the pronounced biofilm structures as revealed by the lectins [18]. In some cases nucleic acid stains SybrGreen/Syto 9 were used for counter-staining. The lectins, which react with *Acidianus* sp. DSM 29099 biofilms and EPS, were found to give constant binding within the test period (not shown). As shown in **Figure 5**, cells attached on pyrite (shown as green dots) are clearly visible, as revealed by SybrGreen signals. Attached cells are mainly characterized as individual cells covered by surface compounds/EPS containing mannose and glucose, as indicated by the presence of Con A signals. After 24 h incubation, several 'cell-like' signals, as judged by Con A binding, but without SybrGreen signals, were often detected (Figure 5, day 1). These nucleic acid free areas of the size of bacteria most likely correspond to 'microbial footprints'. These are remaining cell surface compounds after cell detachment [50, 51]. This phenomenon was also observed if cells were stained by the lectin AAL-A488 (Figure 6A, B). The data suggest that surface glycoconjugates rich in fucose, mannose and

glucose residues are likely to be involved in cell attachment to, and interactions with, pyrite. As the biofilm density increased with time, a few nucleic acid free 'cells' were observed (Figures 5B, C). Up to 25% of the pyrite surface was associated with a monolayer biofilm after 4 d cultivation. A further increase of the biofilm cell density within 1 month of cultivation was not observed (not shown). Interestingly, large pyrite surface areas remained uncolonized, but several were found to be covered by fucose rich compounds as indicated by the presence of AAL-A488 signals (Figure 6C). Cells of *Acidianus* sp. DSM 29099 were detected on the pyrite surface after 5 h of contact (not shown). In addition, cells were often found to be 'vibrating' and seemed to be trapped in a gel-like matrix (Supplementary Movie S1).

In **Figure 7**, EFM images display the distribution of biofilm cells stained with Syto 9, as well as some glycoconjugates of the EPS matrix stained with Con A (Figures 7A, B). AFM scanning revealed structures of the pyrite surface as well as cell and biofilm features. Cells were distributed heterogeneously on the pyrite surface often forming microcolonies. In addition, cells of *Acidianus* sp. DSM 29099 were attached mostly along specific sites (e.g. crystal boundaries) of the pyrite surfaces (Figure 7). This was also observed by CLSM after staining the samples with the lectin AAL (**Figure 8**). In addition, in the presence of cells, the pyrite surface exhibited several corrosion sites (pits) (Figure 7 and Supplementary Fig. S4). In abiotic experiments of pyrite leaching with 5 mM ferric chloride such phenomena were not observed (Supplementary Fig. S4). Thus, it seems that pyrite dissolution by cells of *Acidianus* sp. DSM 29099 is not fully identical with the chemical action of ferric ions only, although ferric ions are in both cases the only oxidizing agent.

EPS production and chemical composition

Two EPS fractions, namely capsular EPS and colloidal EPS of planktonic cells of *Acidianus* sp. DSM 29099 grown with iron(II) ions or pyrite, were obtained via extraction with EDTA. In addition, EPS from biofilms on pyrite were also extracted and analyzed. As shown in **Table 1**, the contents of carbohydrates, uronic acids and proteins in the capsular EPS of iron(II)-grown cells amounted to 27.7, 0.9, and 32.8 mg/10¹² cells, respectively. The total amount of colloidal EPS was 4 times lower than that of capsular EPS. Also, the amount of colloidal EPS from pyrite-grown cells was 5 times lower than the capsular EPS. In addition, no proteins were detected in the colloidal EPS of iron(II)-grown cells. Uronic acids were detected in both capsular EPS and colloidal EPS of pyrite-grown cells in amounts of 8.2 and 5.6 mg/10¹² cells, respectively. However, these amounts were significantly reduced in the EPS of iron(II)-grown cells. The total amount of EPS (capsular plus colloidal EPS) from pyrite-grown cells was 4.3 times higher than that of iron(II)-grown ones. This indicates that the presence of pyrite induced EPS production, which has been reported also for the bacteria *At. ferrooxidans* and *L. ferrooxidans* [12, 30, 49]. In both cases (i.e. cells grown with iron(II) ions or pyrite), the amount of carbohydrate in the colloidal EPS was always higher than the amount of protein (Table 1). The latter was increased in the capsular EPS fractions (Table 1). A low content of protein in the bulk solution (colloidal EPS) has been reported also for the AMD biofilms dominated by *Leptospirillum* group II [52], for *S. metallicus* grown on S⁰ [19], and also for *S. solfataricus*, *S. acidocaldarius* and *S. tokodaii* grown on glucose or casamino acids [53]. However, cells of *Sulfolobales* contain a surface layer, which consists mainly of protein. This may explain why a relatively high amount of protein in the capsular EPS was detected.

Interestingly, small amounts of sulfate were detected in the capsular EPS extracted from cells from both cell populations, if grown with iron(II) ions (0.02 mg/10¹² cells), pyrite (0.07

mg/10¹² cells) or biofilm cells grown on pyrite (0.04 mg/g pyrite). Sulfate has been found in exopolysaccharides of two *Sulfolobus* strains MT3 and MT4 [54]. It is therefore possible that some glycoproteins of *Acidianus* sp. DSM 29099 are sulfated.

The EPS of biofilms on pyrite contained proteins and carbohydrates in amounts of 38.4 mg/g and 18 mg/g pyrite, respectively. The total amount of biofilm EPS produced by *Acidianus* sp. DSM 29099 on pyrite was approximately twice the sum of capsular EPS and colloidal EPS of pyrite-grown planktonic cells. Thus, it seems that a substantial amount of EPS produced by cells of *Acidianus* sp. DSM 29099 was associated with pyrite. This finding is also in agreement with our CLSM observations. Often smear-like EPS were detected on pyrite surfaces (Figure 6C). These may have a role in the microbe-pyrite interactions and in the pyrite dissolution process.

Thus, the EPS of *Acidianus* sp. DSM 29099 grown on iron or pyrite contain mainly carbohydrates, proteins and a small portion of uronic acids. Proteins and carbohydrates are the main EPS components. The EPS amount and components vary according to the growth substrate (iron or pyrite) or lifestyle (planktonic or biofilm). This indicates that protein and carbohydrates are both important for biofilm formation and that these may be the main compounds interacting with pyrite.

The dynamic process of biofilm development of Acidianus sp. DSM 29099

According to our results and previous studies, we propose a model for the biofilm growth by *Acidianus* sp. DSM 29099 on pyrite (**Figure 9**). In the first stage (24-48 h) reversible attachment to the mineral surface is possible, accompanied by the production of adhesive EPS compounds; a limited number of cells attach to the pyrite surface. Chemotaxis due to attraction

to gradients of iron(II)/(III)-ions, thiosulfate and other compounds and possibly mediation by cell appendages may occur [55]. Cell surface compounds containing uronic acids, glucose, mannose and fucose mediate the contact with pyrite surfaces. In stage II: cells are firmly attached and colonize pyrite surfaces; small micro-colonies develop and may also connect with each other by EPS or cell appendages. In addition, pyrite degradation in form of pits can be detected. Large parts of the pyrite surface remain uncolonized, but smear EPS devoid of cells appear. In this stage, cells on the pyrite surface are often associated with defects and crack sites (Figures 7, 8). In stage III, large colonies of up to 50 μm in diameter have formed and corrosion pits can be observed. Along with surface corrosion, cells are embedded in EPS layers, which are mainly composed of carbohydrate and protein. Still, parts of the pyrite surface remain uncolonized by cells. However, most parts are covered by an EPS matrix containing fucose. It is possible that this smear layer may be distributed continuously on the pyrite surface, as shown for other leaching bacteria [30]. The EPS thickness and richness shown by binding of the lectin AAL are probably underestimated, due to the fact that currently no multi-function fluorescent stain is available to label all EPS matrix components [24]. Future work shall investigate the role of EPS components and cell appendages during the biofilm formation process. In addition, genetic manipulation of mutant strains shall be developed to characterize the molecular mechanisms of biofilm formation and development. Nevertheless, it remains a huge challenge to apply this technique to acidophilic microorganisms [56-58].

Conclusions

Biofilm formation on pyrite by *Acidianus* sp. DSM 29099 is a dynamic process accompanied by the production of adhesive compounds, which after cell detachment remain as footprints. Cell surface compounds rich in glucose, mannose and fucose play roles in the initial and

possibly irreversible attachment. EPS, which contain mainly protein and carbohydrate associated with planktonic cell surfaces or associated with biofilms on mineral surfaces, seem to mediate cell-cell and cell-pyrite interactions. The findings will improve the understanding of the specific physiology and metabolic strategies of thermoacidophiles in bioleaching environments. Furthermore, understanding of the thermophilic bioleaching process including cell mineral interactions will be facilitated.

Acknowledgements

We thank U. Kuhlicke (Department of River Ecology, Helmholtz Centre for Environmental Research – UFZ, Magdeburg) for technical support with CLSM. Dr. L. Castro (Department of Material Science and Metallurgical Engineering, Complutense University of Madrid, Madrid) and Dr. Mariia Bellenberg (National Academy of Sciences of Ukraine, Kiev) are acknowledged for help with electron microscopy. M.V. Acknowledges the support by FONDECYT grant 1161007. In particular, we acknowledge the reviewers for the critical and constructive suggestions.

References

- [1] Brierley CL, Brierley JA. Progress in bioleaching: part B: applications of microbial processes by the minerals industries. *Appl Microbiol Biotechnol* 2013;97:7543-52.
- [2] Kaksonen AH, Boxall NJ, Gumulya Y, Khaleque HN, Morris C, Bohu T, *et al.* Recent progress in biohydrometallurgy and microbial characterisation. *Hydrometallurgy* 2018;180:7-25.
- [3] Schippers A. Microorganisms involved in bioleaching and nucleic acid-based molecular methods for their identification and quantification. In: *Microbial Processing of Metal Sulfides* (Donati E, Sand W editors). *Microbial Processing of Metal Sulfides*. Netherlands: Springer 2007, pp. 3-33.
- [4] Vera M, Schippers A, Sand W. Progress in bioleaching: fundamentals and mechanisms of bacterial metal sulfide oxidation—part A. *Appl Microbiol Biotechnol* 2013;97:7529-41.
- [5] Petersen J, Dixon D. Thermophilic heap leaching of a chalcopyrite concentrate. *Miner Eng* 2002;15:777-85.
- [6] Norris PR, Burton NP, Clark DA. Mineral sulfide concentrate leaching in high temperature bioreactors. *Miner Eng* 2013;48:10-19.
- [7] Flemming H-C, Wingender J, Szewzyk U, Steinberg P, Rice SA, Kjelleberg S. Biofilms: an emergent form of bacterial life. *Nat Rev Microbiol* 2016;14:563-75.
- [8] Flemming H-C, Wingender J. The biofilm matrix. *Nat Rev Microbiol* 2010;8:623-33.
- [9] Sheng G-P, Yu H-Q, Li X-Y. Extracellular polymeric substances (EPS) of microbial aggregates in biological wastewater treatment systems: a review. *Biotechnol Adv* 2010;28:882-94.
- [10] Diao M, Taran E, Mahler S, Nguyen AV. A concise review of nanoscopic aspects of bioleaching bacteria–mineral interactions. *Adv Colloid Interface Sci* 2014;212:45-63.
- [11] Li Q, Sand W. Mechanical and chemical studies on EPS from *Sulfobacillus thermosulfidooxidans*: From planktonic to biofilm cells. *Colloids Surf B Biointerfaces* 2017;153:34-40.
- [12] Gehrke T, Telegdi J, Thierry D, Sand W. Importance of extracellular polymeric substances from *Thiobacillus ferrooxidans* for bioleaching. *Appl Environ Microbiol* 1998;64:2743-47.
- [13] Edwards KJ, Bond PL, Gihring TM, Banfield JF. An archaeal iron-oxidizing extreme acidophile important in acid mine drainage. *Science* 2000;287:1796-99.

- [14] Wheaton G, Counts J, Mukherjee A, Kruh J, Kelly R. The confluence of heavy metal biooxidation and heavy metal resistance: Implications for bioleaching by extreme thermoacidophiles. *Minerals* 2015;5:397-451.
- [15] Koerdt A, Jachlewski S, Ghosh A, Wingender J, Siebers B, Albers S-V. Complementation of *Sulfolobus solfataricus* PBL2025 with an α -mannosidase: effects on surface attachment and biofilm formation. *Extremophiles* 2012;16:115-25.
- [16] Jachlewski S, Jachlewski WD, Linne U, Bräsen C, Wingender J, Siebers B. Isolation of extracellular polymeric substances from biofilms of the thermoacidophilic archaeon *Sulfolobus acidocaldarius*. *Front Bioeng Biotechnol* 2015;3:123.
- [17] Neu TR, Kuhlicke U. Fluorescence lectin bar-coding of glycoconjugates in the extracellular matrix of biofilm and bioaggregate forming microorganisms. *Microorganisms* 2017;5:5.
- [18] Zhang R, Neu T, Bellenberg S, Kuhlicke U, Sand W, Vera M. Use of lectins to in situ visualize glycoconjugates of extracellular polymeric substances in acidophilic archaeal biofilms. *Microb Biotechnol* 2015;8:448-61.
- [19] Zhang R, Neu TR, Zhang Y, Bellenberg S, Kuhlicke U, Li Q, *et al.* Visualization and analysis of EPS glycoconjugates of the thermoacidophilic archaeon *Sulfolobus metallicus*. *Appl Microbiol Biotechnol* 2015;99:7343-56.
- [20] Castro C, Zhang R, Liu J, Bellenberg S, Neu TR, Donati E, *et al.* Biofilm formation and interspecies interactions in mixed cultures of thermo-acidophilic archaea *Acidianus* spp. and *Sulfolobus metallicus*. *Res Microbiol* 2016;167:604-12.
- [21] Liu J, Li Q, Sand W, Zhang R. Influence of *Sulfobacillus thermosulfidooxidans* on initial attachment and pyrite leaching by thermoacidophilic archaeon *Acidianus* sp. DSM 29099. *Minerals* 2016;6.
- [22] Zhang R, Bellenberg S, Neu TR, Sand W, Vera M. The biofilm lifestyle of acidophilic metal/sulfur-oxidizing microorganisms. In: *Biotechnology of extremophiles* (Rampelotto PH ed.). *Biotechnology of extremophiles*. Cham: Springer 2016, pp. 177-213.
- [23] Mangold S, Harneit K, Rohwerder T, Claus G, Sand W. Novel combination of atomic force microscopy and epifluorescence microscopy for visualization of leaching bacteria on pyrite. *Appl Environ Microbiol* 2008;74:410-15.
- [24] Neu TR, Lawrence JR. Innovative techniques, sensors, and approaches for imaging biofilms at different scales. *Trends Microbiol* 2015;23:233-42.
- [25] Mackintosh M. Nitrogen fixation by *Thiobacillus ferrooxidans*. *J Gen Microbiol* 1978;105:215-18.

- [26] Aljanabi SM, Martinez I. Universal and rapid salt-extraction of high quality genomic DNA for PCR-based techniques. *Nucleic Acids Res* 1997;25:4692-93.
- [27] Ding J, Zhang R, Yu Y, Jin D, Liang C, Yi Y, *et al.* A novel acidophilic, thermophilic iron and sulfur-oxidizing archaeon isolated from a hot spring of Tengchong, Yunnan, China. *Braz J Microbiol* 2011;42:514-25.
- [28] Schippers A, Jozsa P, Sand W. Sulfur chemistry in bacterial leaching of pyrite. *Appl Environ Microbiol* 1996;62:3424-31.
- [29] Maulani N, Li Q, Sand W, Vera M, Zhang R. Interactions of the extremely acidophilic archaeon *Ferroplasma acidiphilum* with acidophilic bacteria during pyrite bioleaching. *Appl Environ Biotechnol* 2016;1:43-55.
- [30] Harneit K, Göksel A, Kock D, Klock J-H, Gehrke T, Sand W. Adhesion to metal sulfide surfaces by cells of *Acidithiobacillus ferrooxidans*, *Acidithiobacillus thiooxidans* and *Leptospirillum ferrooxidans*. *Hydrometallurgy* 2006;83:245-54.
- [31] Castro L, Zhang R, Muñoz JA, González F, Blázquez ML, Sand W, *et al.* Characterization of exopolymeric substances (EPS) produced by *Aeromonas hydrophila* under reducing conditions. *Biofouling* 2014;30:501-11.
- [32] Dubois M, Gilles KA, Hamilton JK, Rebers P, Smith F. Colorimetric method for determination of sugars and related substances. *Anal Chem* 1956;28:350-56.
- [33] Blumenkrantz N, Asboe-Hansen G. New method for quantitative determination of uronic acids. *Anal Biochem* 1973;54:484-89.
- [34] Bradford MM. A rapid and sensitive method for the quantitation of microgram quantities of protein utilizing the principle of protein-dye binding. *Anal Biochem* 1976;72:248-54.
- [35] Ng FM, Dawes EA. Chemostat studies on the regulation of glucose metabolism in *Pseudomonas aeruginosa* by citrate. *Biochem J* 1973;132:129-40.
- [36] Dunk R, Mostyn R, Hoare H. The determination of sulfate by indirect atomic absorption spectroscopy. *At Absorpt Newsletter* 1969;8:79-81.
- [37] Giaveno MA, Urbietta MS, Ulloa JR, Toril EG, Donati ER. Physiologic versatility and growth flexibility as the main characteristics of a novel thermoacidophilic *Acidianus* strain isolated from Copahue geothermal area in Argentina. *Microb Ecol* 2013;65:336-46.
- [38] Goris J, Konstantinidis KT, Klappenbach JA, Coenye T, Vandamme P, Tiedje JM. DNA–DNA hybridization values and their relationship to whole-genome sequence similarities. *Int J Syst Evol Microbiol* 2007;57:81-91.
- [39] Konishi Y, Yoshida S, Asai S. Bioleaching of pyrite by acidophilic thermophile *Acidianus brierleyi*. *Biotechnol Bioeng* 1995;48:592-600.

- [40] Larsson L, Olsson G, Holst O, Karlsson HT. Pyrite oxidation by thermophilic archaeobacteria. *Appl Environ Microbiol* 1990;56:697-701.
- [41] Gehrke T, Hallmann R, Kinzler K, Sand W. The EPS of *Acidithiobacillus ferrooxidans* - a model for structure-function relationships of attached bacteria and their physiology. *Water Sci Technol* 2001;43:159-67.
- [42] Zhu W, Xia J-L, Yang Y, Nie Z-Y, Peng A-A, Liu H-C, *et al.* Thermophilic archaeal community succession and function change associated with the leaching rate in bioleaching of chalcopyrite. *Bioresour Technol* 2013;133:405-13.
- [43] Castro C, Donati E. Effects of different energy sources on cell adhesion and bioleaching of a chalcopyrite concentrate by extremophilic archaeon *Acidianus copahuensis*. *Hydrometallurgy* 2016;162:49-56.
- [44] Xia JL, Zhu HR, Wang L, Liu HC, Nie ZY, Zhao YD, *et al.* In situ characterization of relevance of surface microstructure and electrochemical properties of chalcopyrite to adsorption of *Acidianus manzaensis*. *Adv Mat Res* 2015;1130:183-87.
- [45] Bromfield L, Africa C-J, Harrison S, Van Hille R. The effect of temperature and culture history on the attachment of *Metallosphaera hakonensis* to mineral sulfides with application to heap bioleaching. *Miner Eng* 2011;24:1157-65.
- [46] Africa C-J, van Hille RP, Sand W, Harrison STL. Investigation and *in situ* visualisation of interfacial interactions of thermophilic microorganisms with metal-sulphides in a simulated heap environment. *Miner Eng* 2013;48:100-07.
- [47] Fröls S, Dyllal - Smith M, Pfeifer F. Biofilm formation by haloarchaea. *Environ Microbiol* 2012;14:3159-74.
- [48] Urbietta MS, Rascovan N, Castro C, Revale S, Giaveno MA, Vazquez M, *et al.* Draft genome sequence of the novel thermoacidophilic archaeon *Acidianus copahuensis* strain ALE1, isolated from the Copahue volcanic area in Neuquén, Argentina. *Genome Announc* 2014;2:e00259-14.
- [49] Bellenberg S, Leon-Morales C-F, Sand W, Vera M. Visualization of capsular polysaccharide induction in *Acidithiobacillus ferrooxidans*. *Hydrometallurgy* 2012;129-130:82-89.
- [50] Neu TR, Marshall KC. Microbial “footprints”—a new approach to adhesive polymers. *Biofouling* 1991;3:101-12.
- [51] Neu TR. Microbial "footprints" and the general ability of microorganisms to label interfaces. *Can J Microbiol* 1992;38:1005-08.

- [52] Jiao Y, Cody GD, Harding AK, Wilmes P, Schrenk M, Wheeler KE, *et al.* Characterization of extracellular polymeric substances from acidophilic microbial biofilms. *Appl Environ Microbiol* 2010;76:2916-22.
- [53] Ellen AF, Albers S-V, Driessen AJ. Comparative study of the extracellular proteome of *Sulfolobus* species reveals limited secretion. *Extremophiles* 2010;14:87-98.
- [54] Nicolaus B, Manca MC, Ramano I, Lama L. Production of an exopolysaccharide from two thermophilic archaea belonging to the genus *Sulfolobus*. *FEMS Microbiol Lett* 1993;109:203-06.
- [55] Edwards KJ, Bond PL, Banfield JF. Characteristics of attachment and growth of *Thiobacillus caldus* on sulphide minerals: a chemotactic response to sulphur minerals? *Environ Microbiol* 2000;2:324-32.
- [56] Orell A, Fröls S, Albers S-V. Archaeal biofilms: the great unexplored. *Annu Rev Microbiol* 2013;67:337-54.
- [57] Díaz M, Castro M, Copaja S, Guiliani N. Biofilm formation by the acidophile bacterium *Acidithiobacillus thiooxidans* involves c-di-GMP pathway and Pel exopolysaccharide. *Genes* 2018;9:113.
- [58] van Wolferen M, Orell A, Albers SV. Archaeal biofilm formation. *Nat Rev Microbiol* 2018;16:699-713.

Figure and Table legends

Fig. 1. Morphology of cells of *Acidianus* sp. DSM 29099 grown on S^0 (A) or pyrite (B and C) visualized by AFM (A), SEM (B) and TEM (C). The arrows (solid line) in A and B indicate a typical lobe-shaped appearance of *Sulfolobales* and arrows (dotted line) in A and C show surface compounds/excretions of cells, respectively.

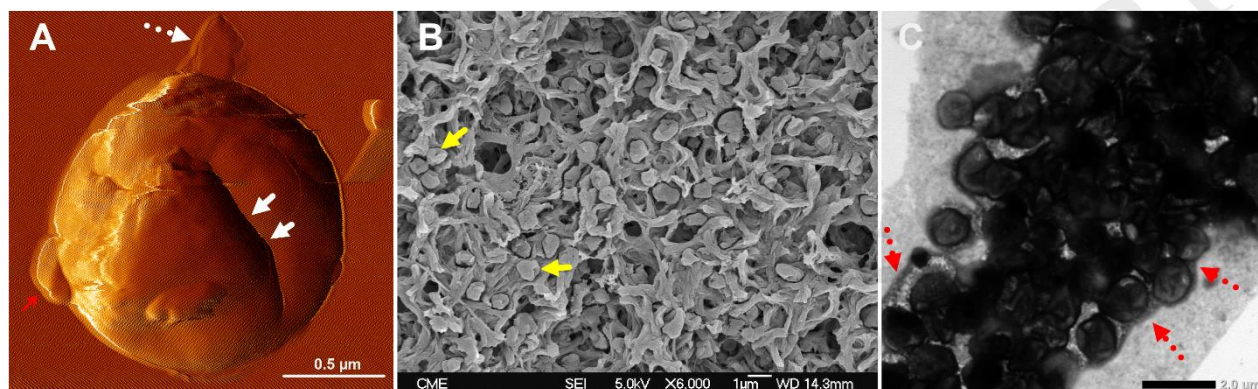


Fig. 2. Growth of *Acidianus* sp. DSM 29099 in MAC medium with iron(II) ions at 65°C and shaking at 120 rpm.

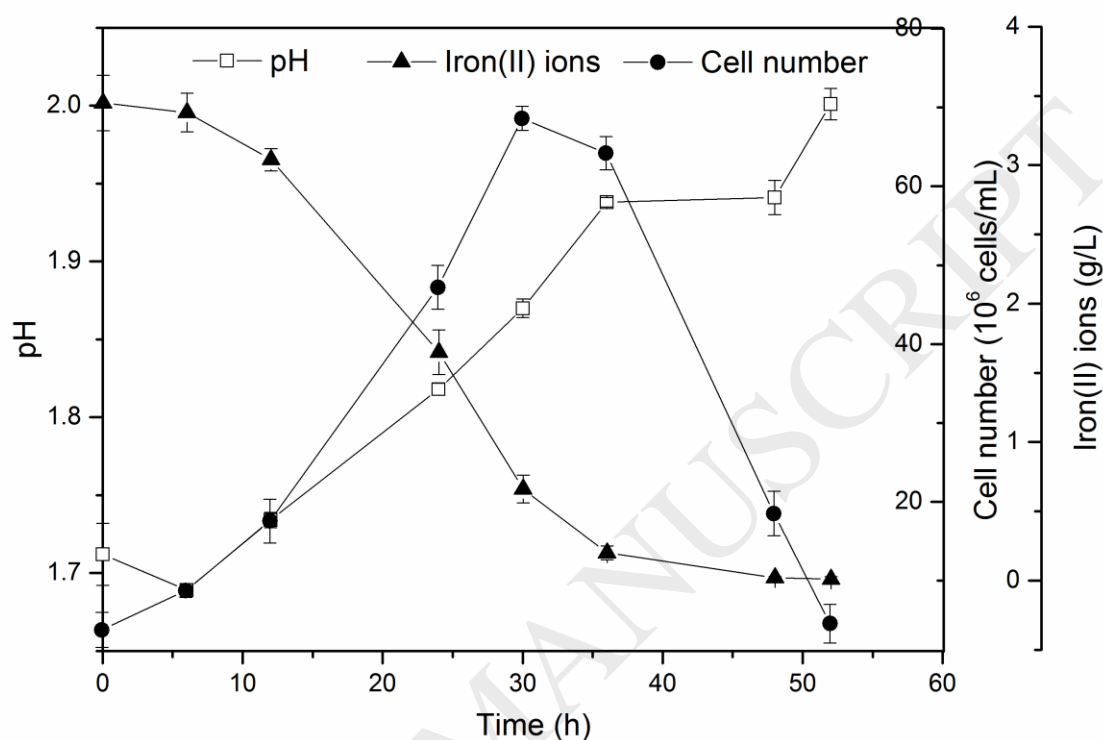


Fig. 3. Bioleaching of pyrite by cells of *Acidianus* sp. DSM 29099 (square symbols) or *S. metallicus* (triangle symbols). Experiments were carried out in flasks containing 100 MAC medium with 10% pyrite and 0.02% yeast extract at 65°C and 120 rpm.

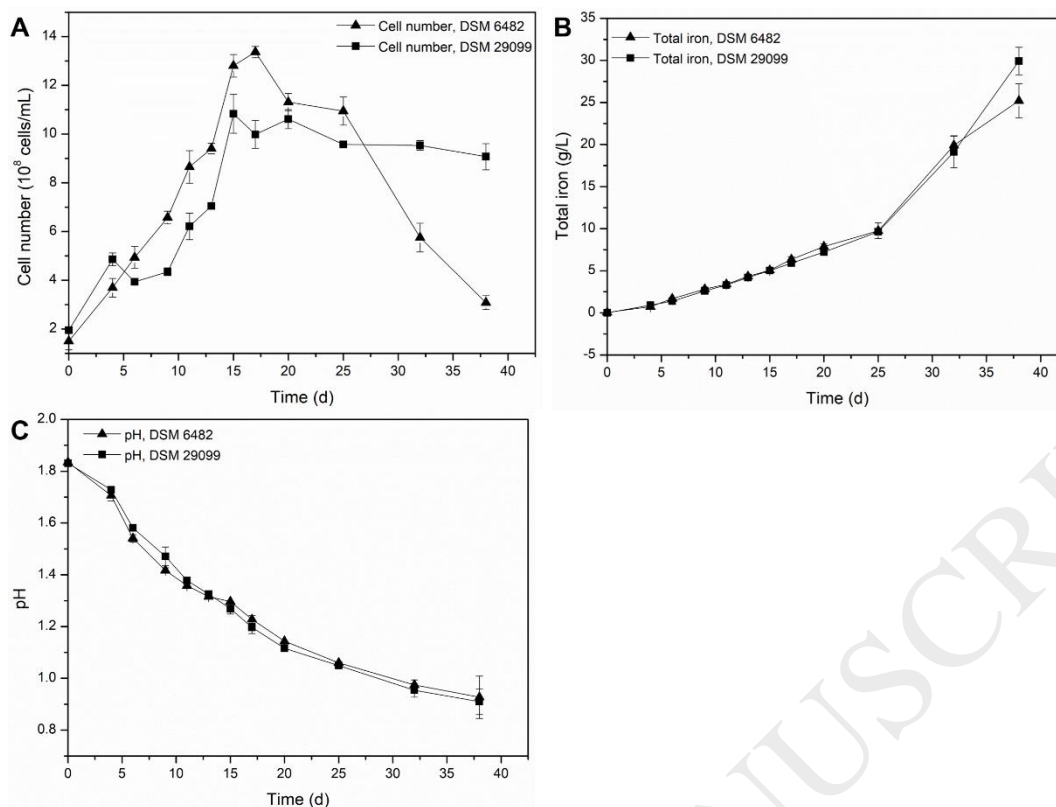


Fig. 4. Attachment of *Acidianus* sp. DSM 29099 cells to pyrite, chalcopyrite or quartz. Cells ($1-2 \times 10^8$ cells/ml) were inoculated with 20% of pyrite, chalcopyrite and quartz. Cells were cultivated at 65 °C and shaking at 120 rpm.

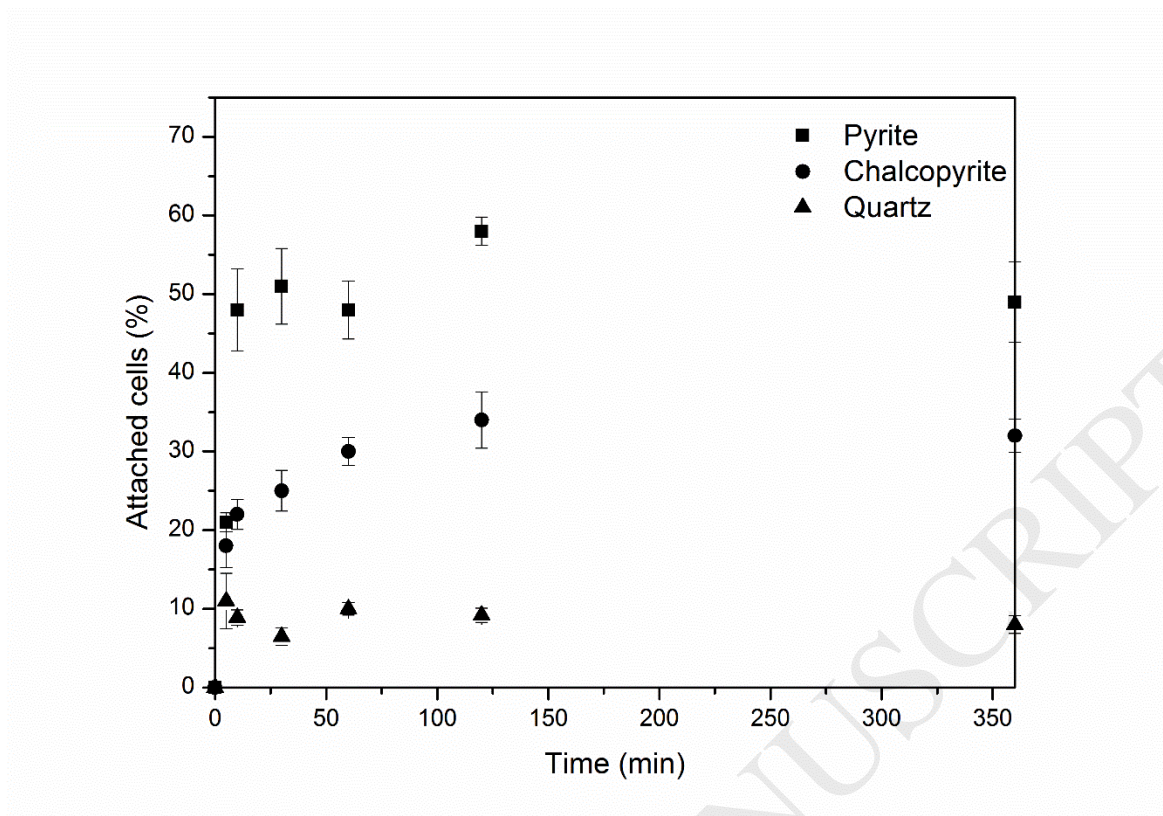


Fig. 5. Biofilm development of *Acidianus* sp. DSM 29099 on pyrite slices (shining side) after 1 day (upper row), 2 days (middle row) and 4 days (bottom row) cultivation. Biofilm cells were stained by binding of Con A-TRITC (red) and SybrGreen (green). Pyrite surface is shown in the overlay as reflection signal (=grey). Arrows indicate ‘cells’ free of nucleic acids also known as microbial footprints.

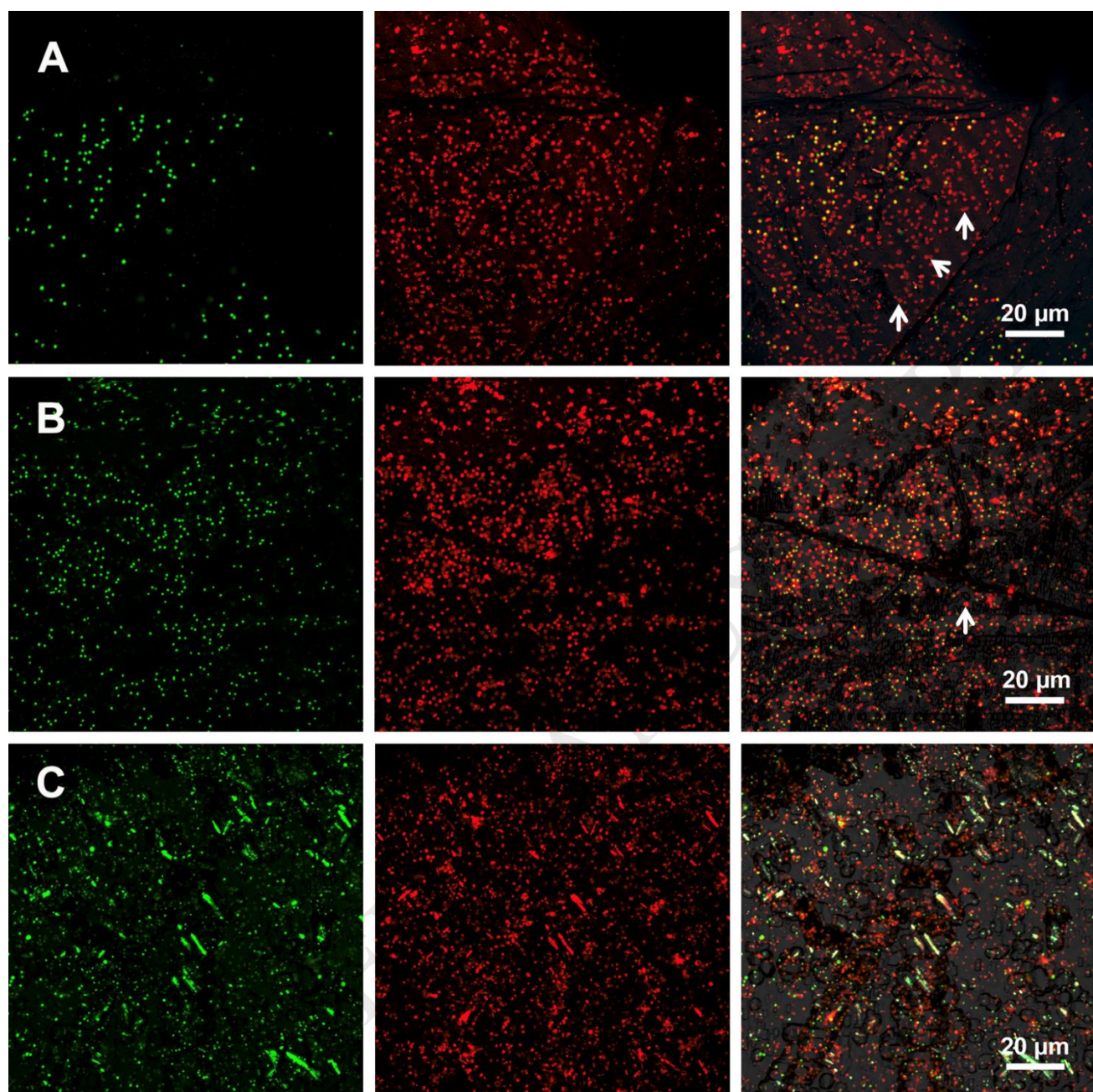


Fig. 6. Biofilms of *Acidianus* sp. DSM 29099 on pyrite after 1 day (A and B) and 7 days (C) of cultivation. Biofilm cells were stained by AAL-A488 (green). The pyrite surface is shown as reflection signal (grey). Arrows in B indicate cell EPS/surface compounds containing fucose left over by detached cells as footprints. White arrows in C indicate smear AAL signals derived from cells which spread on pyrite surface and above microcolonies.

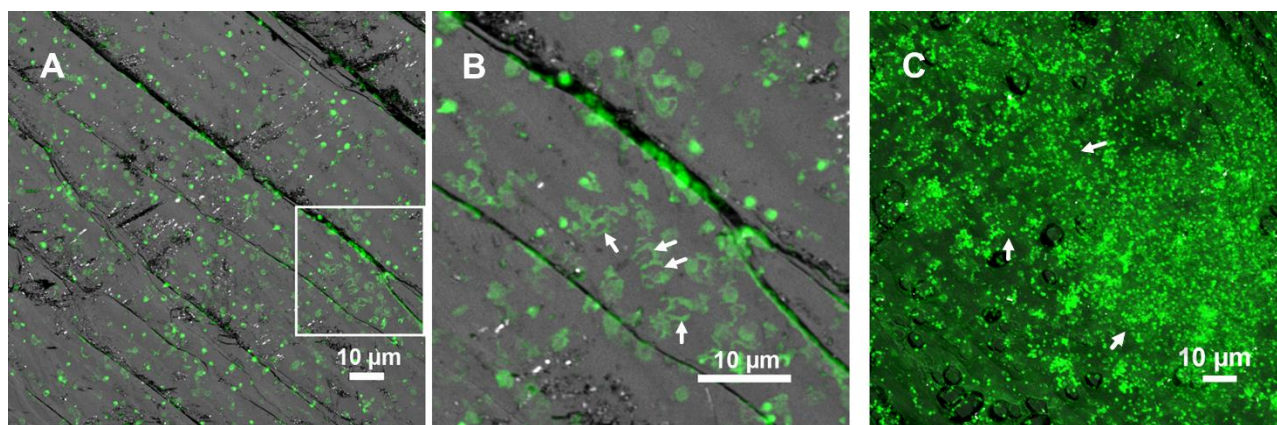


Fig. 7. Biofilm cells of *Acidianus* sp. DSM 29099 visualized by AFM combined with epifluorescence microscopy, exhibiting preferential attack on the pyrite lattice along planes. A and B show EFM images of *Acidianus* sp. DSM 29099 biofilms stained by Syto 9 (green) and Con A-TRITC (red), respectively. C shows AFM images corresponding to epifluorescence microscopy (A and B). White dashed ovals indicate cell aggregations along pyrite defective sites. Blue arrows show a single cell on pyrite. Bars=10 µm.

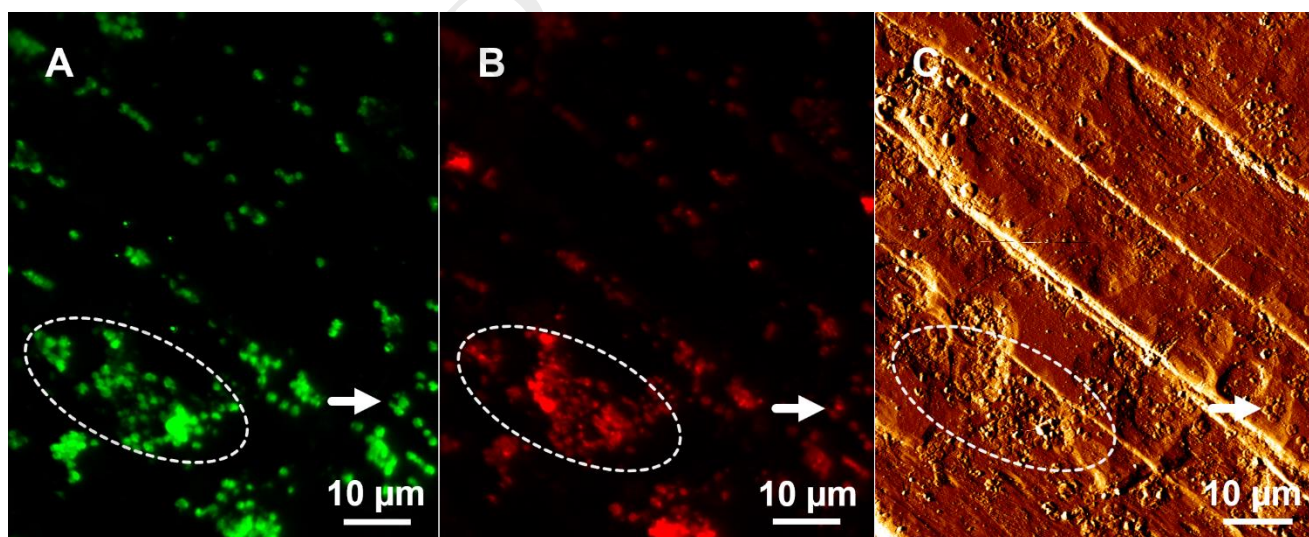


Fig. 8. Biofilms of *Acidianus* sp. DSM 29099 on pyrite. The images of the same data set show in three different projections the preference for growth along pyrite surface structures. Top: maximum intensity projection, middle: transparent 3D projection, bottom: iso-surface projection. Cells were stained by AAL-A488 (green). Pyrite is shown as reflection (grey).

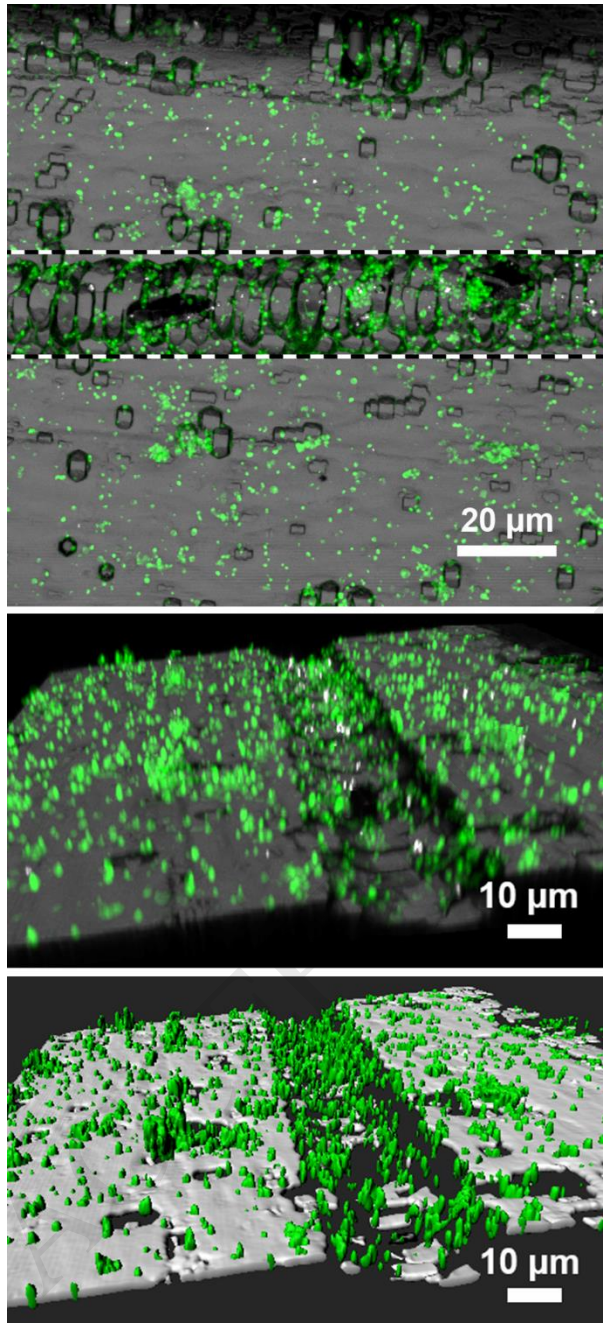


Fig. 9. Proposed mode of biofilm development by *Acidianus* sp. DSM 29099 on pyrite. The biofilm development can be divided into three stages. Stage I: initial attachment. Stage II: irreversible attachment. Stage III: biofilm maturation. a, b (CLSM images), and c (AFM image) are accompanying the model for biofilm formation.

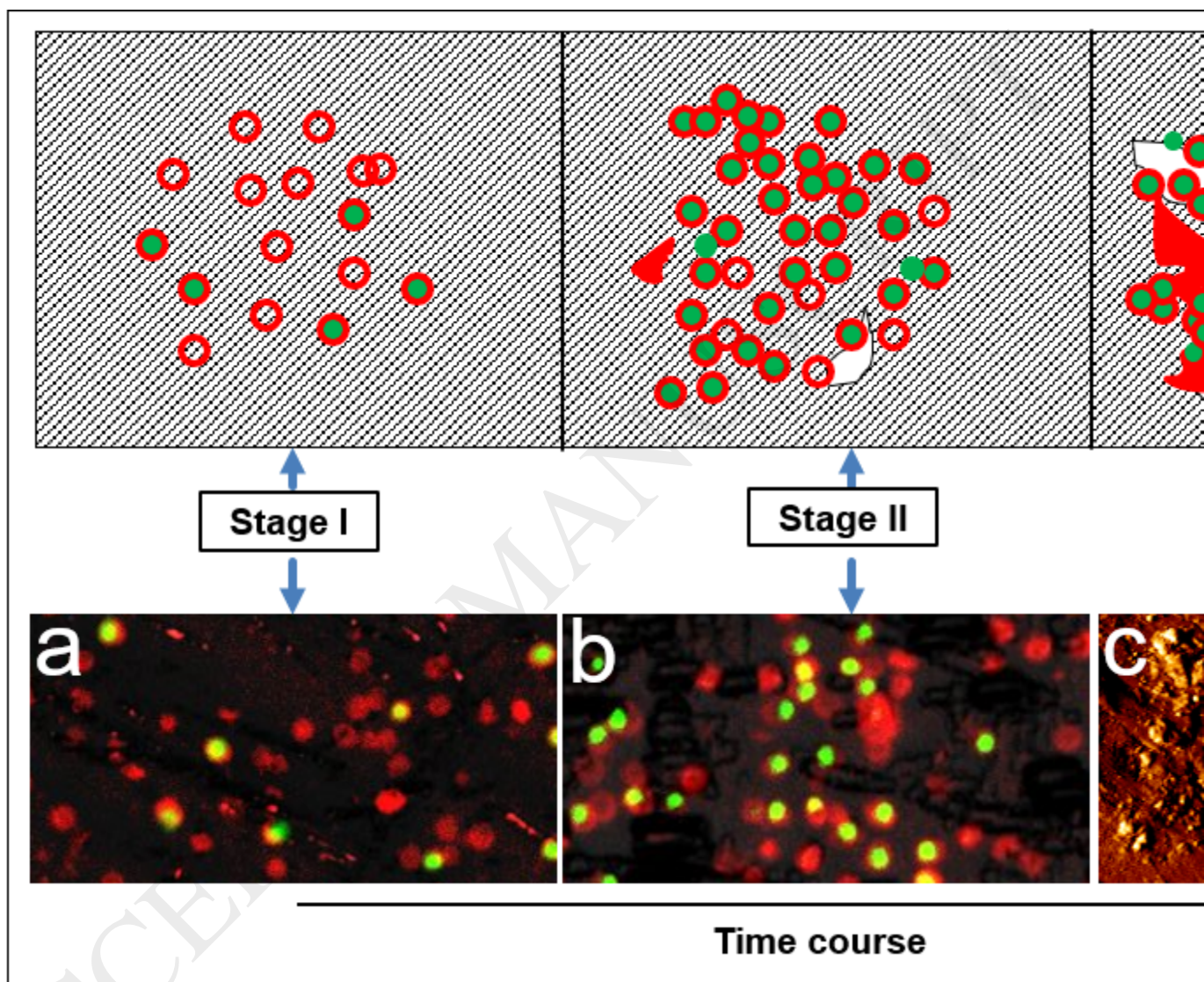


Table 1. EPS composition of *Acidianus* sp. DSM 29099 after growth with different energy substrates

Substrate	EPS type	Carbohydrate	Uronic acid	Protein	Sulfate	G6PDH*
Iron(II)	Capsular ^a	27.7±3.9	0.9±0.1	32.8±5	0.02±0.01	<4 %
	Colloidal ^a	14.2±1	0.02±0.01	BL	BL	ND
Pyrite	Capsular ^a	80.2±12.5	8.2±3.5	182.6±28	0.07±0.04	<2 %
	Colloidal ^a	39.3±3	5.6±0.2	7.4±0.6	BL	ND
	Biofilms on pyrite ^b	18±2.6	4.7±0.6	38.4±2.6	0.04±0.01	ND

a: mg/10¹² cells. b: mg/g pyrite.

*: percentage of G6PDH activity from EPS samples accounts for the G6PDH activity from whole cell biomass.

BL: Below detection limit

ND: Not determined